Available online at www.sciencedirect.com

ScienceDirect

Proceedings of the Combustion Institute 36 (2017) 4193–4200

Proceedings of the Combustion Institute

www.elsevier.com/locate/proci

Self-sustained catalytic combustion of carbon monoxide ignited by dielectric barrier discharge

Feng Bin [a], Xiaolin Wei [a], Teng Li [a,*], Deliang Liu [b], Qinglan Hao [b], Baojuan Dou [b,**]

[a] *State Key Laboratory of High-Temperature Gas Dynamics, Institute of Mechanics, Chinese Academy of Science, Beijing 100190, PR China*

[b] *College of Marine & Environmental Sciences, Tianjin University of Science & Technology, Tianjin 300457, PR China*

Received 3 December 2015; accepted 28 June 2016
Available online 14 July 2016

Abstract

This paper presents the results of a study of self-sustained catalytic combustion of CO ignited by dielectric barrier discharge (DBD) using $Ce_{0.5}Zr_{0.5}O_y/TiO_2$ (CeZr/Ti), $CuZr_{0.25}O_y/TiO_2$ (CuZr/Ti), and $CuCe_{0.75}Zr_{0.25}O_y/TiO_2$ (CuCeZr/Ti) catalysts. DBD excites and dissociates some of the reactant molecules in the gas phase. These are more easily adsorbed on the catalyst surface than are ground-state species, therefore induction begins at a lower background temperature than in thermal catalysis. CO is adsorbed on copper sites, therefore CeZr/Ti is inactive in CO ignition, but CuZr/Ti and CuCeZr/Ti achieve DBD ignition at 34 and 44 s, respectively, at a specific energy density (SED) of 1500 J/L. CO catalytic ignition by DBD involves two steps. The induction process is dominated by plasma catalysis. At the same SEDs, induction with CuCeZr/Ti begins earlier than those with CuZr/Ti, in good agreement with the reducibilities and oxygen-transfer properties of these catalysts. The ignition process is governed by thermal catalysis because the enhancement of external diffusion induced by increasing the temperature improves the reaction rate. CuZr/Ti provided more CO adsorption sites than did CuCeZr/Ti, contributing to shortening of the ignition delay.

Keywords: Self-sustained catalytic combustion; Carbon monoxide; Ignition; Dielectric barrier discharge

1. Introduction

The off-gas produced during basic oxygen furnace steelmaking contains a considerable amount of CO. Because a high concentration of oxygen in combination with CO is liable to cause explosions, the off-gas generated at steelmaking intermissions is not directly recovered as a fuel, and is often discharged into the atmosphere via conventional flare burners [1]. Our new method for using this energy in CO catalytic oxidation is based on methane self-sustained catalytic combustion as an alternative route for electric power generation. In this process, a mixture of methane and O_2 generates

* Corresponding author. Fax: +86 10 82544222.
** Corresponding author. Fax: +86 22 60600300.
E-mail addresses: Tengli@imech.ac.cn, liteng@imech.ac.cn (T. Li), bjdou@tust.edu.cn (B. Dou).

http://dx.doi.org/10.1016/j.proci.2016.06.181
1540-7489

local hot spots on the catalyst surface, and then adjacent methane and O_2 molecules are dissociated, leading to a thermochemical runaway reaction, followed by self-sustained non-flame burning [2]. Such a combustion strategy is suitable for portable electricity generation, because of its high combustion efficiency in small-scale devices.

Dielectric barrier discharge (DBD)-assisted ignition and oxidation processes have recently drawn attention because they give rapid start-up under cold conditions [3]. This involves strong coupling of electron-induced chemistry and thermochemistry. Discharge produces electronic excitation, dissociation, and ionization of molecules, followed by plasma chemical reactions, and the background temperature increase not only induces thermochemical reactions, but also affects the plasma physics. Zhang et al. [4] identified the contributions of the effects of plasma chemistry and thermochemistry, and confirmed that the reactant conversions depend on both two processes by independently controlling the temperature and the reactor pressure, whereas the consecutive reactions depend mainly on the temperature and the corresponding thermo-chemistry. Mintusov et al. [5] reported that the temperature increase in air–C_2H_4 flows is caused by exothermic plasma chemical oxidation, which results in ignition when the flow temperature approaches the auto-ignition temperature. Jo et al. [6] found that the ratio of the plasma power to the heating input power is an important parameter for enhancing methane oxidation. The results can be characterized by limitedness, however, due to their methodology of a high-temperature plasma source and a narrow temperature range. Although many reports have linked plasma-assisted ignition of air–fuel flows, no statistical evidence of plasma-assisted catalytic ignition to achieve self-sustained combustion has yet been presented.

Our previous study showed that $CuCe_{0.75}Zr_{0.25}O_y$ mixed oxides formed on ZSM-5 substrates show excellent catalytic activities because copper–ceria synergism improves the redox capability and the ceria–zirconium solid solution has a good oxygen storage capacity [7]. In this work, we achieved CO self-sustained combustion ignited by DBD for the first time, using $CuCe_{0.75}Zr_{0.25}O_y/TiO_2$ (CuCeZr/Ti), $CuZr_{0.25}O_y/TiO_2$ (CuZr/Ti), and $Ce_{0.75}Zr_{0.25}O_y/TiO_2$ (CeZr/Ti) catalysts with Cu:Ce:Zr molar ratios of 1:0.75:0.25. Inert TiO_2 was used as the substrate because of its excellent thermal stability and good dispersion of active species. The promotion of active phase dispersion, oxygen mobility, and redox properties caused by strong interactions among copper, cerium, and zirconium species will be discussed. We distinguished between the effects of electron-induced chemistry and thermochemistry by using DBD and temperature-programmed ignition (TPI), combined with various characterization techniques. The results obtained will be helpful in introducing the use of plasma-assisted ignition for self-sustained catalytic combustion of CO in steelmaking off-gas.

2. Experimental specifications

2.1. Synthesis of catalysts

The TiO_2 support was pure anatase TiO_2 (Degussa). The CuCeZr/Ti, CuZr/Ti, and CeZr/Ti catalysts were prepared using an incipient wetness impregnation method. The TiO_2 gel support was impregnated with an aqueous solution containing appropriate amounts of copper, zirconium, and cerium nitrates. The catalysts were dried for 8 h at 120 °C and calcined in air for 6 h at 600 °C. The dried samples were crushed and sieved to 10–12 mesh. The copper content of the CuCeZr/Ti catalyst was fixed at 4 wt% and the molar ratio of Cu:Ce:Zr was 1:0.75:0.25. For the CuZr/Ti and CeZr/Ti catalysts, the molar ratios of Cu:Zr and Ce:Zr were 1:0.25 and 0.75:0.25, respectively.

2.2. Characterization

X-ray photoelectron spectroscopy (XPS) was performed using a Kratos Axis Ultra DLD spectrometer with a Mg Kα X-ray source. Temperature-programmed H_2 reduction (H_2-TPR) experiments were performed using a Micromeritics 2920 II instrument with 5% H_2/Ar at a heating rate of 15 °C/min to 600 °C. Prior to reduction, the sample (ca. 200 mg) was pretreated in flowing Ar at 300 °C for 1 h. Temperature-programmed O_2 desorption (O_2-TPD) was also performed with the Micromeritics 2920 II instrument using 200 mg of sample. After O_2 (30 mL/min) saturation for 1 h, the gas was switched to Ar for 0.5 h, and TPD was performed by ramping the temperature at 10 °C/min to 600 °C in Ar (30 mL/min). Desorption of O_2 was detected using a thermal conductivity detector. In situ diffuse-reflectance infrared Fourier-transform (DRIFT) spectroscopy was performed using a Bruker Tensor 27 spectrophotometer. Self-supporting disks prepared from the sample powders were suspended in a quartz holder and then mounted in an IR cell (Tianjin XianQuan Industry and Trade Development CO., Ltd.) connected to a vacuum line. The disks were heated at 300 °C in N_2 for 1 h and evacuated to a pressure of 3×10^{-3} mbar for 1 h. The IR CO adsorption measurements were performed at CO pressures of about 20 Torr with the samples at room temperature. After exposure to CO, IR spectra were recorded at 30 s intervals until the spectrum was stable.

2.3. Experimental setup

Figure 1 shows a schematic diagram of the experimental setup. The system consisted of a continuous flow gas-supply system, electric furnace,

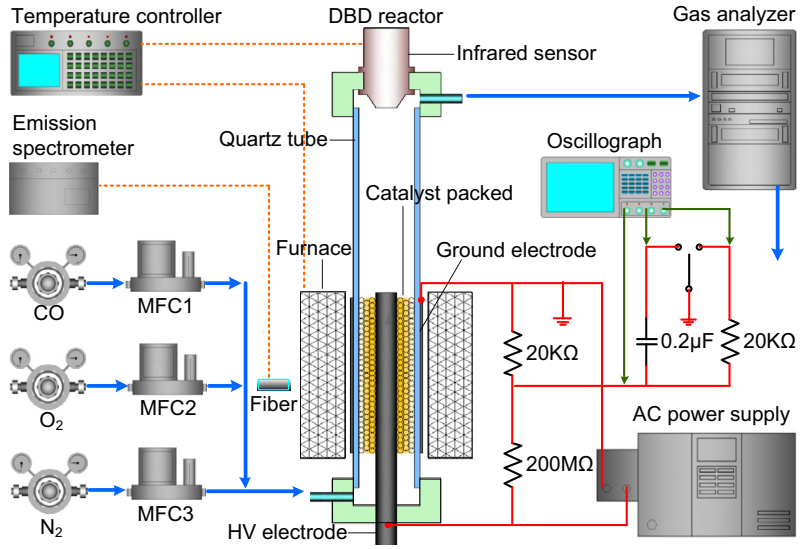

Fig. 1. Schematic diagram of experimental setup.

electric and gaseous analytical systems, AC power supply (1–50 kHz, 0–30 kV, sine wave), and a DBD reactor. The feed gas contained 15% CO and balance 15% O_2/N_2, and the flow rate was 3 L/min. An online gas analyzer (Maihak) was used to monitor the effluent CO, O_2, NO_x, and CO_2.

The plasma was generated in a tubular quartz reactor of inner diameter 15 mm and wall thickness 1.5 mm, which acted as a dielectric and separated the inner and outer electrodes. A cerium–tungsten rod of diameter 8 mm was selected as the inner electrode, which was connected to a high voltage and placed on the axis of the reactor. Steel-wire netting (length 5 cm) was wrapped around the outer surface of the quartz as the grounding electrode. A plasma zone was created between the inner electrode and the dielectric, which was packed with catalyst. An emission spectrometer (USB2500 PLUS, Ocean Optics) connected by an optical fiber to an optical access facility was used to identify the reactive species generated during DBD. The distance between the optical fiber and the discharge zone was about 5 mm. The catalyst background temperature during discharge was measured using an IR temperature sensor along the inner axis. Before TPI was performed by ramping the temperature at 10 °C/min, the quartz reactor was mounted in a tube furnace and the reaction temperature was controlled based on the measurements made by the IR temperature sensor.

Electrical discharge measurements were performed using a digital oscilloscope (Tektronix, TDS1102). The applied voltage was determined using a 10,000:1 divider resistor connected in parallel with the discharge circuit, and the current was obtained from the voltage drop across a 20 kΩ sampling resistor connected in series with the ground electrode of the DBD reactor. The consumed energy and capacitance of the adjacent dielectric barrier were estimated from voltage–charge Lissajous figures, using a 0.2 μF non-inductive capacitor inserted between the reactor and the ground instead of the sampling resistor [8]. The specific energy density (SED) was calculated as the consumed energy divided by the total flow rate.

3. Results and discussion

3.1. XPS analysis

The chemical states and surface compositions of the catalysts were investigated using XPS. The Cu 2p spectra (Fig. 2a) for the CuCeZr/Ti and CuZr/Ti catalysts show two main peaks, for Cu $2p_{3/2}$ and Cu $2p_{1/2}$, at about 933.0 and 953.8 eV, respectively. The shake-up peaks located in the range 938.1–947.7 eV confirm the presence of divalent copper. Peak deconvolution and fitting split the Cu $2p_{3/2}$ peak into two peaks, at 932.6 and 934.4 eV, corresponding to Cu^+ and Cu^{2+} ions, respectively. The Ce 3d spectra of the catalysts (Fig. 2b) were individually deconvoluted into $3d_{5/2}$ and $3d_{3/2}$ spin–orbit components (labeled v and u, respectively), which arise from $Ce^{4+} \leftrightarrow Ce^{3+}$ electronic transitions. The main chemical valence of cerium in the CuCeZr/Ti and CeZr/Ti catalysts is +4 (v, v_2, v_3, u, u_2, and u_3), but a small quantity of Ce^{3+} (v_1 and u_1) is also present (Table 1). Enhancement of the homogeneities of the cerium and zirconium atoms promotes the $Ce^{4+} \rightarrow Ce^{3+}$ valence change, because of substitution of Ce^{4+} by Zr^{4+} during calcination.

Table 1
Surface atomic ratios of catalysts obtained from XPS analysis.The bulk atomic ratios are listed in the bracket.

Sample	Cu/Ti	Cu^{2+}/Cu^{+}	Ce/Ti	Ce^{3+}/Ce^{4+}
CuCeZr/Ti	0.235 (0.059)	1.68	0.082 (0.044)	0.319
CuZr/Ti	0.224 (0.055)	2.06	/	/
CeZr/Ti	/	/	0.104 (0.042)	0.758

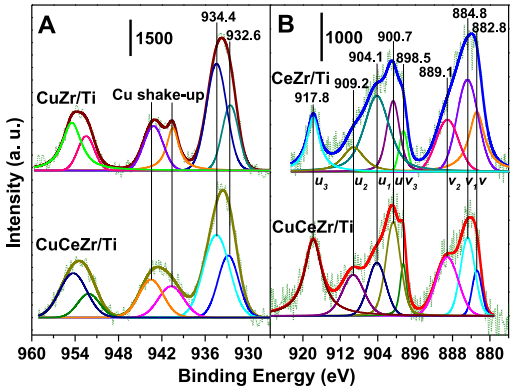

Fig. 2. Narrow Cu 2p (A) and Ce 3d (B) XP spectra of catalysts.

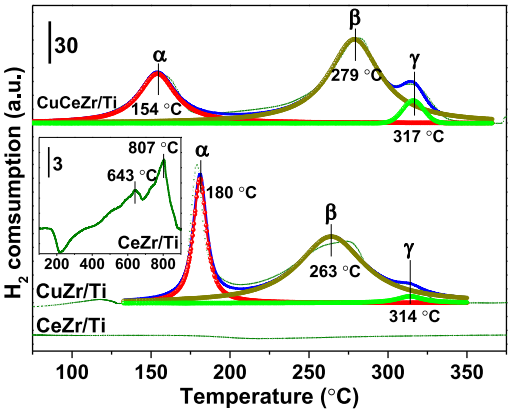

Fig. 3. H_2-TPR profiles of catalysts.

The surface composition atomic ratios of Cu/Ti and Ce/Ti determined using XPS are presented in Table 1 along with the corresponding bulk ratios listed in parentheses. The ratios obtained using XPS are about four times higher than the corresponding bulk values, indicating that copper and cerium tend to migrate to the surfaces of TiO_2 grains. The Cu^{2+}/Cu^{+} ratio decreases significantly from 2.06 for CuZr/Ti to 1.68 for CuCeZr/Ti. This result is in agreement with those reported by Gaudin et al. [9] and indicates that the presence of cerium oxide favors the formation of Cu^{+} species. Quantitative data give Ce^{3+}/Ce^{4+} ratios of 0.319 for CuCeZr/Ti and 0.758 for CeZr/Ti. The presence of Ce^{3+} in the catalysts favors the formation of vacancies and unsaturated chemical bonds on the surface, resulting in increased oxygen adsorption [10].

3.2. H_2-TPR analysis

The redox properties of the catalysts were investigated using H_2-TPR. Figure 3 shows that CeZr/Ti does not give distinct reduction peaks in the range 50–400 °C and undergoes reduction with two temperature maxima, at 643 and 807 °C, arising from reduction of surface Ce^{4+} ions. In the cases of CuZr/Ti and CuCeZr/Ti, three reduction peaks, at 154–180 (α-H_2), 263–279 (β-H_2), and 314–317 °C (γ-H_2), are observed in the TPR profiles. The α and β peaks are associated with small and medium-sized CuO particles, which are highly dispersed on the catalyst surface and have reduction temperatures significantly lower than that of bulk CuO (γ peak). For CuZr/Ti, the α peak appears within a narrow temperature range (160–210 °C), because of local temperature runaway. This observation is in accordance with the high Cu^{2+}/Cu^{+} ratio for CuZr/Ti detected by XPS. The position of the α peak shifts to lower temperature for CuCeZr/Ti, and those of the β and γ peaks shift to higher ones. The β and γ peak shifts clearly result from the growth of small and medium-sized CuO particles after cerium addition. The α peak shift suggests enhanced catalyst reducibility and can be correlated with structural changes in the catalyst, because copper species preferentially interact with ceria to form Cu–Ce solid solutions. The total amount of H_2 consumed during a H_2-TPR run was 42.2 μmol/g for CuCeZr/Ti, i.e., higher than that of 39.6 μmol/g for CuZr/Ti. It is probable that some copper ions enter the ceria lattice, and this increases the oxygen mobility and enables easy reduction of copper [11].

3.3. CO adsorption at room temperature

DRIFT spectra of CO adsorbed on the catalysts are shown in Fig. 4. There is no CO chemisorption peak in the region 2200–2000 cm^{-1} for CeZr/Ti, but there is a faint band at 2144 cm^{-1} corresponding to weak physisorption. The strong band at 2109 cm^{-1} for the CuCeZr/Ti and CuZr/Ti catalysts is assigned to CO adsorption at copper sites to form Cu^{+}–carbonyls, because the d orbitals of copper

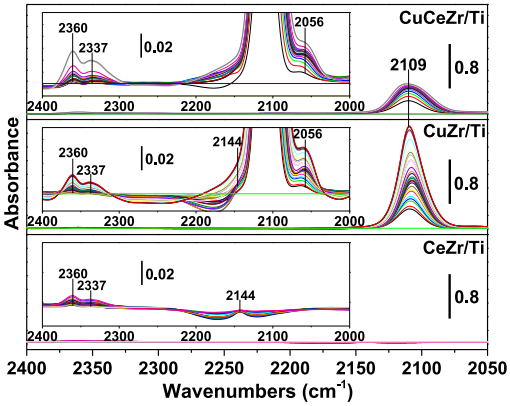

Fig. 4. DRIFT spectra of CO adsorbed on catalysts.

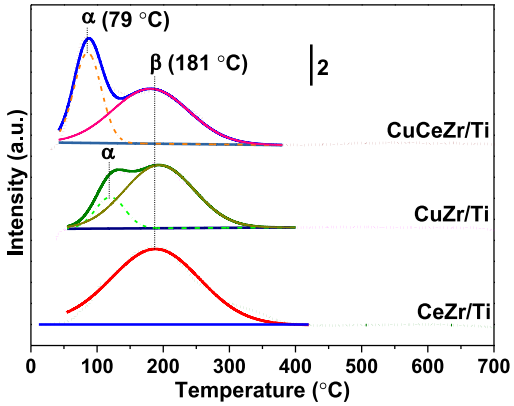

Fig. 5. O_2-TPD profiles of catalysts.

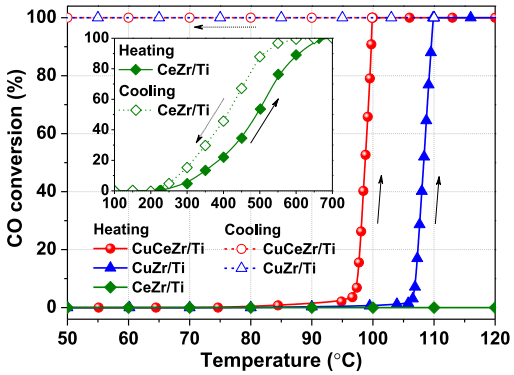

Fig. 6. Temperature-programmed ignition of CO over catalysts.

ions are completely or nearly full, and can form strong bonds with CO. The cerium ions, however, with the outer shell electron distributions of 4f1 and 5S2 4d10 5P6, respectively, are difficult to offer electrons from d-orbitals to the anti-bonding π-orbitals. The affinity between cerium and CO is therefore weak. Such chemisorption giving rise to Cu^+–carbonyl species would occur when Cu^{2+} species (insert toward CO adsorption) are automatically reduced to Cu^+ in the starting catalysts [12].

A comparison of the DRIFT spectra of CuCeZr/Ti and CuZr/Ti shows that the intensity of the Cu^+–carbonyl band for CuZr/Ti is significantly higher than that for CuCeZr/Ti, which is in accordance with the Cu^{2+}/Cu^+ ratio of CuZr/Ti being higher than that of CuCeZr/Ti, as shown by XPS. The weak band at 2056 cm^{-1} is assigned to CO linearly adsorbed on Cu^0, which is unstable and does not contribute to CO oxidation. CO_2 signals at 2337 and 2360 cm^{-1} can also be monitored. The faint reaction between Cu^+–carbonyls and lattice oxygen in the catalysts at room temperature explain this behavior.

3.4. Temperature-programmed O_2 desorption

O_2-TPD tests were performed to confirm oxygen activation over the catalysts. Figure 5 shows that CuZr/Ti and CuCeZr/Ti give α and β desorption peaks, but CeZr/Ti gives only a β desorption peak. Considering the low desorption temperature (<350 °C), the active oxygen species are probably O_2^- [13]. The lower-temperature α-oxygen desorption can be related to copper species dispersed on the catalyst surface, whereas β-oxygen desorption results from copper- and/or cerium-impregnated ZrO_2. The Ce 3d XP spectra show that oxygen vacancies are present in the cerium-containing catalysts, therefore the formation of α-oxygen species in CuCeZr/Ti via oxygen vacancies in copper–cerium mixed oxides is plausible. The larger peak area and lower desorption peak temperature for CuCeZr/Ti show that its α-oxygen adsorption capacity is higher than that of CuZr/Ti, indicating that oxygen is easily activated by CuCeZr/Ti.

3.5. Temperature-programmed catalytic ignition of CO

Before investigating the effects of DBD on CO catalytic ignition, the activities of CeZr/Ti, CuZr/Ti, and CuCeZr/Ti were evaluated using TPI tests, with data from the heating and cooling steps in the experiments. The results are shown in Fig. 6. On heating, CeZr/Ti is inactive in CO combustion until the temperature is greater than 228 °C. CO conversion gradually increases with increasing temperature and reaches 100% at 683 °C. The cooling process occurs at lower temperatures than the corresponding heating process, showing hysteresis, because of exothermic oxidation reactions. For CuZr/Ti and CuCeZr/Ti, significant catalytic ignition can occur at the gas–solid phase interface, giving CO ignition temperatures (T_{ig}, corresponding to 10% CO conversion) of 106 and 97 °C, respectively. The high low-temperature

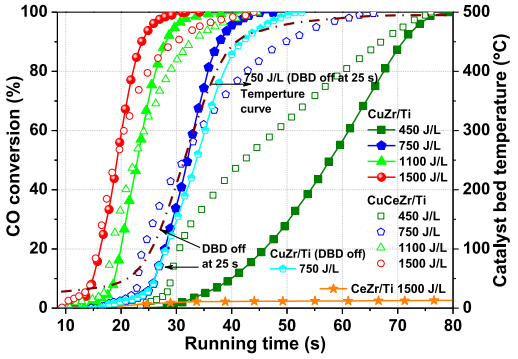

Fig. 7. CO catalytic ignition induced by DBD.

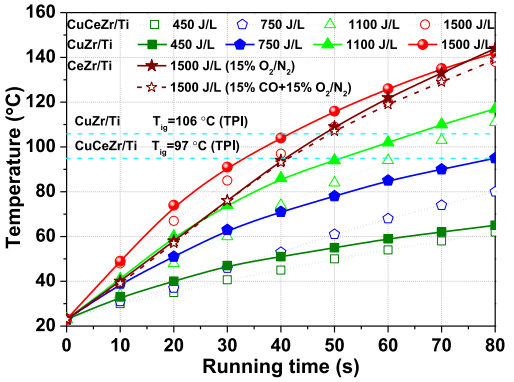

Fig. 8. Background temperature evolution with time as function of DBD. Gas conditions: 15% CO + 15% O_2/N_2 and 15% O_2/N_2 for CeZr/Ti; 15% O_2/N_2 for CuZr/Ti and CeCeZr/Ti.

activity over CuCeZr/Ti is related to incorporation of some copper ions into cerium oxides and the formation of a Ce^{4+}/Ce^{3+} redox couple, which promotes reducibility and facilitates oxygen transport on the catalyst surface (shown by H_2-TPR and O_2-TPD). Under cooling, 100% CO conversion can be consistently maintained, even after the controlled temperature decreases to room temperature, i.e., around 25 °C. Fast mass and heat transfer at the gas–solid phase interface clearly promote self-sustained CO catalytic combustion.

3.6. Catalytic ignition of CO by DBD

Application of an AC voltage to a CO + O_2/N_2 mixture causes electrical breakdown at about 6.5 kV (AC frequency = 10.0 kHz, room temperature). Figure 7 shows the effects of DBD on CO catalytic ignition. The supplied voltage was varied to obtain SEDs from 450 to 1500 J/L, which is similar to that (0.5–2.0 kJ/L) of Subrahmanyam et al. [14] and that (0.2–1.7 kJ/L) of Kiwi-Minsker et al. [15]. The high SED is employed in the present work in order to shorten the ignition time of CO catalytic combustion. CO clearly cannot be ignited by DBD over the CeZr/Ti catalyst, even when the SED is 1500 J/L, which is very similar to that for TPI. The dissociation energy of CO molecules is 13.5 eV, therefore CO molecule dissociation is difficult, but they can collide with active oxygen radicals in the gas phase to form small amounts of CO_2. The low CO conversion during discharge does not depend on the temperature and corresponding thermocatalysis, because the CeZr/Ti background temperature, which was monitored synchronously (Fig. 8), increased from room temperature to 144 °C after DBD operation for 80 s. These results strongly suggest that the supported copper catalysts play a dominant role in the DBD-assisted ignition of CO. The effects of thermal and plasma catalysis were distinguished by measuring the background temperatures of CuZr/Ti and CuCeZr/Ti in a 15% O_2/N_2 atmosphere instead of 15% CO + 15% O_2/N_2, to avoid runaway induced by CO ignition, since the temperature curves obtained for the CeZr/Ti has only 5 °C difference under these two circumstances till the DBD operation at 80 s (Fig. 8). The current flow induced by the migration of electrons and ions promotes a temperature increase in the reactor through joule heating, dielectric loss, and gas heating in the plasma channel. The temperature rise with time is faster for CuZr/Ti than for CuCeZr/Ti at the same SED. This behavior can be explained by a higher capacitance of the dielectric barrier for CuZr/Ti (Table 2), leading to a higher dielectric loss.

Table 2
Capacitances of dielectric barriers for catalysts during DBD.

Sample	Capacitance of dielectric barrier (nF)			
	450 J/L	750 J/L	1100 J/L	1500 J/L
CeZr/Ti	24.7	32.6	41.7	55.3
CuZr/Ti	21.9	40.7	51.9	62.1
CuCeZr/Ti	25.3	33.2	43.9	55.5

Taking CuZr/Ti as an example, when the SED is set at 450 J/L, micro-discharges are created but a low current density is maintained. In this case, CO oxidation starts at 29 s and gradually increases with DBD operating time up to 100% CO conversion at 79 s (Fig. 7). An increase in the SED significantly reduces the ignition delay, and two main steps occur during DBD. At an SED of 750 J/L, the first step can be described as a slow induction process that begins at 18 s and then continues at a relatively slow rate until 25 s. The reaction rate in this region is controlled by transport of reactants to the active sites on the catalysts [16]. The second step is the ignition process. The oxidation rate at this point is fast enough to induce a strong increase in the local temperature, and then catalytic light-off is propagated because of the evolved reaction heat, even if the DBD is cut off at this stage, as shown in

Fig. 7, enabling thermal CO combustion. Typical temperature curve of catalyst bed as a function of time, with initiation and cessation of DBD, has also been given in Fig. 7. In this step, the reaction rate is controlled by external diffusion [17]. Kirkpatrick et al. [18] showed that the plasma generated upstream of the catalyst gave a thermal "push" to the catalyst when it was near its light-off temperature. Because of the low concentration of CO (0.45%), however, thermochemical runaway did not occur on the catalyst surface. Therefore, only 23% CO conversion was achieved. A combination of the results in Figs. 7 and 8 shows that DBD-assisted catalytic ignition occurs at 27 s (ignition time t_{ig}, determined at 10% CO conversion), corresponding to a background temperature of 60 °C, which is significantly lower than the T_{ig} (97 °C) for thermal catalysis. These results indicate that plasma generates reactive radicals and excited molecules, which may contribute to CO catalytic ignition. At the same SED, the induction process occurs earlier with CuCeZr/Ti than with CuZr/Ti, with t_{ig} values of 23, 17, and 14 s for CuCeZr/Ti at SEDs of 750, 1100, and 1500 J/L, respectively. The ignition curves for the second step, however, show that the increases in CO conversion over CuCeZr/Ti are slower (the slopes are less steep) than those over CuZr/Ti. The ignition curves for CuZr/Ti cross with those for CuCeZr/Ti at 33, 24, and 20 s at SEDs of 750, 1100, and 1500 J/L respectively, and 100% CO conversion is achieved at 47, 42, and 34 s, respectively, which shortens the ignition delay. In DBD ignition, CO_2 is the only product and no other byproducts can be detected.

3.7. Active species generated during DBD

The plasma species present in the DBD discharge were identified from global optical emission spectra recorded in pure N_2, O_2, CO, and 15% CO + 15% O_2/N_2 discharges. The spectra are shown in Fig. 9. In a pure N_2 atmosphere, the main emission peaks in the range 200–390 nm are the N_2 second positive system ($C^3\Pi_u$–$B^3\Pi_g$). In a pure O_2 discharge, O is not detected. The N_2^* emission spectrum arises from gas breakdown outside the reactor. Although the high-energy electrons in DBD can dissociate oxygen molecules into atoms, ozone formation consumes oxygen atoms, e.g., $O(^3P)$ and $O(^1D)$. In the DBD spectrum of CO, the Ångstrom ($B^1\Sigma^+$–$A^1\Pi$) ro-vibrational system appears in the range 515–590 nm, corresponding to highly excited electronic states of CO [19]. For DBD of the CO + O_2/N_2 mixture, the spectral lines of N_2 molecules are more intense than those of other species, because N_2 accounts for 70% of the gas mixture. The presence of N_2 results in a decrease in the CO excitation rate, but some excited N_2^* can collide with O_2 to produce oxygen atoms. This is comparable to O_2 dissociation by collisions with electrons, and results in a higher density of oxygen atoms (328.3 and 394.2 nm) than that in a pure O_2 atmosphere. The rate coefficients for electron-impact dissociations and excitations of N_2, O_2, and CO were calculated based on the electron Boltzmann equation using the standard BOLSIG+ code and the cross-section from the Phelps database [20]. For given discharge conditions (SED of 450–1500 J/L), the reduced electric field ratio E/N (where E is the electric field strength and N is the number of neutral particles) varies from 45 to 135 Td, corresponding to a mean electron energy of 1.1 to 3.5 eV, as shown in Fig. 10. It can be clearly seen that the most efficient channel is dissociation with production of ground-state $O(^3P)$ and excited $O(^1D)$ atoms. The formation rate coefficients of the active species decrease in the sequence: $O(^3P) > O(^1D) > CO^*(A^1\Pi) > N_2^*(B^3\Pi_g) > N_2^*(B^3\Pi_g) > CO^*(B^1\Pi)$. Such active species formed by DBD can promote CO catalytic ignition.

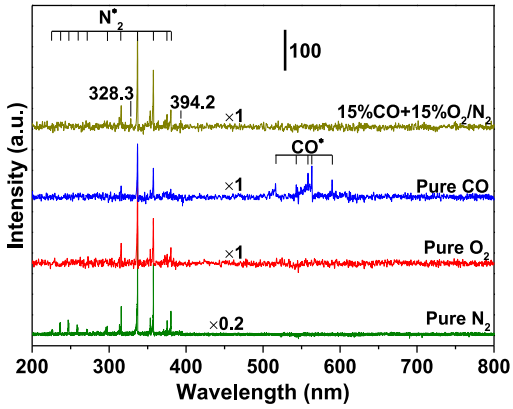

Fig. 9. Optical emission spectra of DBD over CeZr/Ti at SED of 1500 J/L.

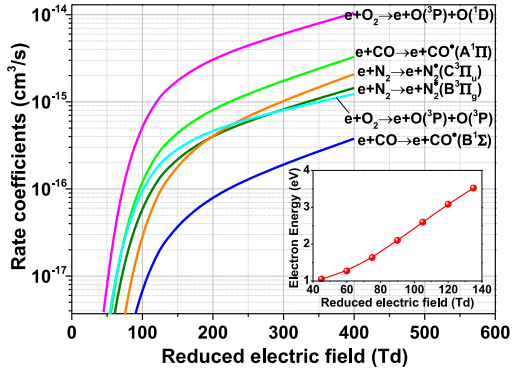

Fig. 10. Rate coefficients of active species formed by direct impact with electrons.

3.8. Proposed reaction mechanism

CO catalytic ignition on CuZr/Ti and CuCeZr/Ti proceeds via a Langmuir–Hinshelwood mechanism, in both plasma and thermal catalysis. During TPI, CO is adsorbed on copper sites in the induction step to yield Cu^{+}–carbonyls, and gaseous O_2 is adsorbed on either copper sites or oxygen vacancies in the mixed oxides. In these competitive adsorption processes, CO adsorption is favored, therefore the reaction is self-poisoned by CO [17]. The critical amount of adsorbed CO can be reached by increasing the temperature to shift the adsorption/desorption equilibrium toward oxygen desorption. At this point, some adsorbed CO also interacts with adsorbed oxygen atoms in a slow exothermic reaction that results in gaseous CO_2 formation and release. When the system is ignited by increasing the temperature, all the adsorbed CO immediately reacts rapidly, and sufficient free adsorption sites are generated frequently for CO adsorption. During DBD, the discharge excites some of the CO molecules and dissociates O_2 molecules into oxygen atoms in the gas phase before adsorption. Given that the molecules delivered to the catalyst surface are already excited or dissociated, the adsorption step is easier, leading to induction beginning at a lower background temperature than in thermal catalysis. At this stage, plasma catalysis is dominant. At the same SED, induction with CuCeZr/Ti begins earlier than that with CuZr/Ti. This is in good agreement with the reducibilities and oxygen-transfer properties of these catalysts. The superiority of CuCeZr/Ti is maintained until the ignition process begins. The CO oxidation rate is fast enough to induce a strong increase in the local temperature, which accelerates external diffusion and mass transfer, based on the gas diffusivity $D_v \propto T^{1.81}$ and the mass-transfer coefficient $K_s = (D_v S)^{1/2}$, where T is temperature and S denotes the update frequency [21]. In this step, external diffusion (thermal catalysis) is dominant. Because more CO adsorption sites can be provided by CuZr/Ti than by CuCeZr/Ti, which is beneficial for external diffusion and mass transfer, the ignition curves for CuZr/Ti cross those for CuCeZr/Ti, contributing to shortening of the ignition delay.

4. Conclusion

We investigated DBD-ignited self-sustained CO combustion over CeZr/Ti, CuZr/Ti, and CuCeZr/Ti catalysts, combined with TPI. DBD ignition gave rapid start-up and evolved in two steps. The induction process was dominated by plasma catalysis. Because of the higher reducibility and oxygen-transfer ability of CuCeZr/Ti, induction was earlier with this catalyst than with CuZr/Ti, the ignition process was governed by thermal catalysis. CuZr/Ti provided more CO adsorption sites than did CuCeZr/Ti, and this helped to shorten the ignition delay.

Acknowledgment

This work is financially supported by the National Natural Science Found of China (No. 21307088). The work is also supported by State Key Laboratory of Engines, Tianjin University (K2014-8).

References

[1] S. Li, X.L. Wei, L.X. Yu, *Fuel* 90 (2011) 1350–1360.
[2] J.E. Abboud, N. Jiang, Z. Zhang, S. Roy, J.R. Gord, *Combust. Flame* 160 (2013) 1842–1847.
[3] S. Nagaraja, W. Sun, V. Yang, *Proc. Combust. Inst.* 35 (2015) 3497–3504.
[4] X. Zhang, M.S. Cha, *Proc. Combust. Inst.* 35 (2015) 3447–3454.
[5] E. Mintusov, A. Serdyuchenko, I. Choi, *Proc. Combust. Inst.* 32 (2009) 3181–3188.
[6] S. Jo, D.H. Lee, Y.-H Song, *Int. J. Hydrog. Energy* 38 (2013) 13643–13648.
[7] S. Li, Q. Hao, R. Zhao, D. Liu, H. Duan, B. Dou, *Chem. Eng. J.* 71 (2013) 939–944.
[8] B. Dou, F. Bin, C. Wang, Q Jia, J. Li, *J. Electrostat.* 71 (2013) 939–944.
[9] P. Gaudin, S. Dorge, H. Nouali, et al., *Appl. Catal. A: Gen.* 504 (2015) 110–118.
[10] Q. Wan, L. Duan, K. He, J. Li, *Chem. Eng. J.* 170 (2011) 512–517.
[11] R. Zhang, W.Y. Teoh, R. Amal, B. Chen, S. Kaliaguine, *J. Catal.* 272 (2010) 210–219.
[12] D. Gamarra, A. Martínez-Arias, *J. Catal.* 263 (2009) 189–195.
[13] Y. Yu, Q. Zhong, W. Cai, J. Ding, *J. Mol. Catal. A: Chem.* 398 (2015) 344–352.
[14] S. Mahammadunnisa, P. Manoj Kumar Reddy, E. Linga Reddy, C. Subrahmanyam, *Catal. Today* 211 (2013) 53–57.
[15] C. Subrahmanyam, A. Renken, L. Kiwi-Minsker, *Appl. Catal. B: Environ.* 65 (2006) 157–162.
[16] K. Arnby, A. Törncrona, B. Andersson, M. Skoglundh, *J. Catal.* 272 (2004) 252–261.
[17] P.-A Carlsson, M. Skoglundh, *Appl. Catal. B: Environ.* 101 (2011) 669–675.
[18] M.J. Kirkpatrick, E. Odic, S. Zinola, J. Lavyb, *Appl. Catal. B: Environ.* (2012) 1–9.
[19] R. Geiger, D. Staack, *J. Phys. D: Appl. Phys.* 44 (2015) 274005.
[20] Plasma Data Exchange Project, *Phelps database*, www.lxcat.net.
[21] W. L.Mccabe, J. C.Smith, Peter Harriott, *Unit Oper. Chem. Eng.* (1993).